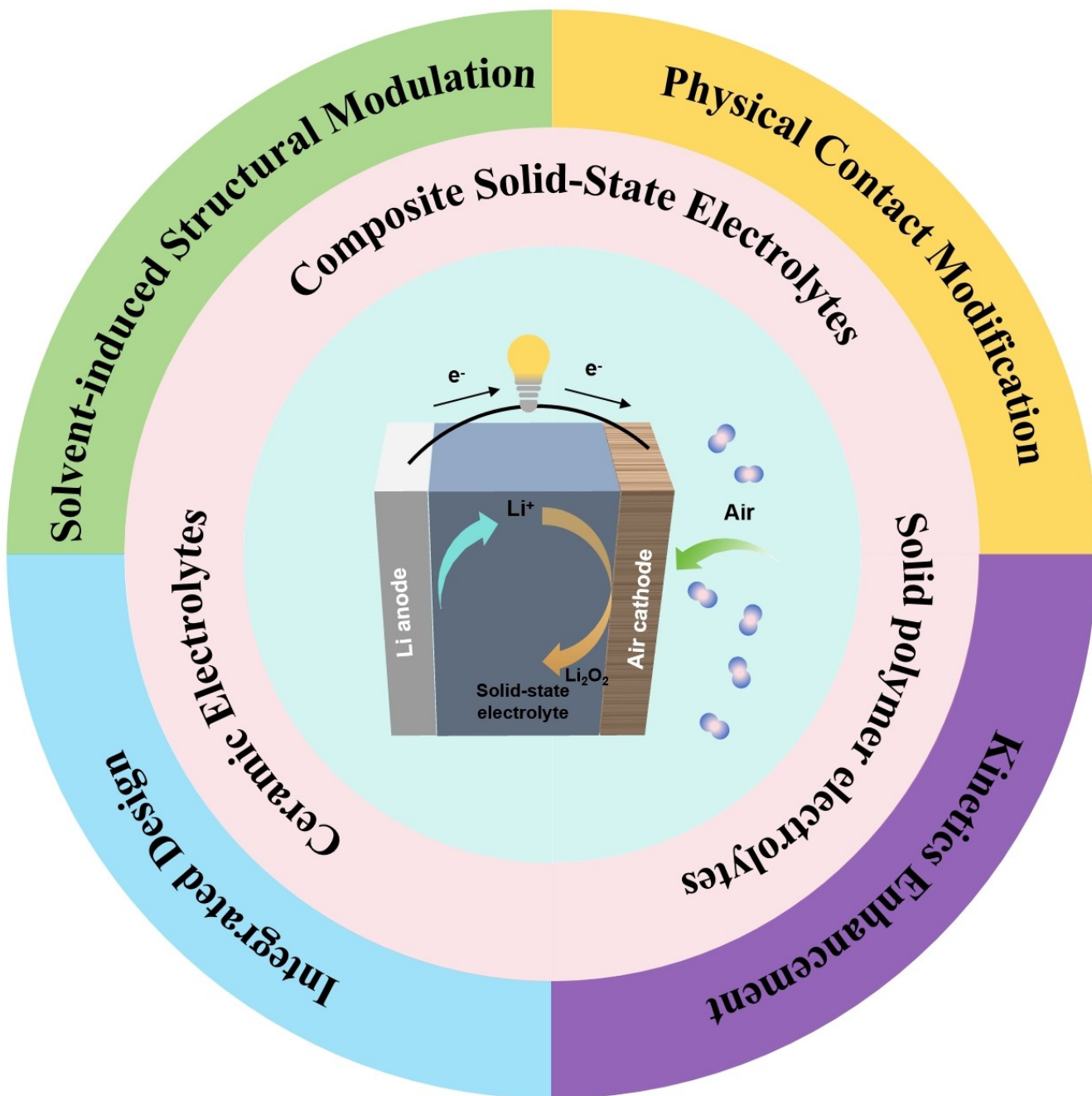


# Solid-State Electrolytes for Lithium-Air Batteries

Xianhai Qi,<sup>[a]</sup> Dapeng Liu,<sup>\*[a]</sup> Haohan Yu,<sup>[a]</sup> Zerui Fu,<sup>[a]</sup> and Yu Zhang<sup>\*[a, b]</sup>



Li-air batteries (LABs) have attracted widespread attention due to their extremely high theoretical capacity and energy density. However, the practical application of liquid-state LABs is substantially hindered by safety concerns, including flammability, leakage, and electrolyte decomposition. In comparison, solid-state electrolytes (SSEs) possess excellent mechanical strength, high safety, good stability, and non-flammable characteristics, offering a feasible strategy for achieving stable and practical

LABs. In this review, we will focus on the development and challenges of solid-state lithium-air batteries (SSLABs), providing an overview of various types of SSEs and discussing the interfacial issues within SSLABs along with potential solutions, and finally propose strategies and outlooks for advanced SSLABs. It is expected that this review will provide a systematic understanding and theoretical framework to guide the design of high-performance SSLABs.

## 1. Introduction

Under the background of continuously growing energy demands, it is of urgency to develop advanced sustainable energy technologies as alternatives to fossil fuels.<sup>[1]</sup> Some new energy technologies have been widely applied in fields such as electric vehicles, renewable energy storage, smart grids, and portable electronic devices due to their clean, efficient, and safe advantages.<sup>[2]</sup> Among the emerging secondary battery systems, Li-air batteries (LABs) are hailed as the “Holy Grail” of next-generation secondary batteries by virtue of their extremely high theoretical energy density (3500 Wh/kg).<sup>[3]</sup> Additionally, LABs utilize oxygen from the air as the cathode material, which enhances material efficiency, reduces costs, and offers significant environmental benefits.<sup>[4]</sup> In the future, LABs, with their unique advantages, are expected to demonstrate significant development potential in areas such as new energy storage.<sup>[5]</sup>

As a semi-open system, LABs are composed of Li anode, air cathode, separator, and electrolyte as shown in Figure 1.<sup>[6]</sup> During discharge, Li is oxidized into  $\text{Li}^+$  at anode, and mean-

while  $\text{O}_2$  accepts electrons to form  $\text{LiO}_2$  and further reacts with  $\text{Li}^+$  to form  $\text{Li}_2\text{O}_2$  at cathode. While during charge,  $\text{Li}_2\text{O}_2$  decomposes into  $\text{Li}^+$  and  $\text{O}_2$ , and  $\text{Li}^+$  is further reduced into Li at anode ( $\text{Li} + \text{O}_2 \leftrightarrow \text{Li}_2\text{O}_2$   $E^\circ = 2.96$  V vs. Li/Li $^+$ ).<sup>[7]</sup> In LABs, electrolytes, as indispensable components, play the crucial role in promoting  $\text{Li}^+$  transport, expanding the electrochemical stability window, suppressing side reactions, and manipulating redox mechanisms.<sup>[8]</sup> The physico-chemical properties and compositions of electrolytes can strongly influence the morphology and distribution of  $\text{Li}_2\text{O}_2$ , and furthermore battery performance and cycle life.<sup>[9]</sup> In addition, the interactions among solvent molecules,  $\text{Li}^+$ , and anions directly determine the solvation structure in electrolyte and thus the construction of inorganic-rich solid-electrolyte interface (SEI) and cathode-electrolyte interphase (CEI).<sup>[10]</sup>

Generally, LABs can be classified into four types by electrolytes, including aqueous, hybrid, non-aqueous, and solid-state ones (Figure 2).<sup>[11]</sup> Aqueous LABs use water as electrolyte and a ceramic membrane to separate Li anode from electrolyte in order to prevent violent reactions between the water and Li metal (Figure 2a). The discharge product of LiOH has high solubility in water, which could deliver a large specific capacity.<sup>[12]</sup> The water-organic hybrid ones use an aqueous electrolyte at cathode and an organic electrolyte at anode (Figure 2b), and the ceramic membrane in the middle acts as a barrier to prevent the water and organic solutions from contact. Additionally, the membrane functions as an ion conduction layer to facilitate  $\text{Li}^+$  transport.<sup>[13]</sup> However, both aqueous and water-organic hybrid LABs often show poor mechanical



Figure 1. Schematic diagram of a typical LAB. Reprinted from Ref. [6] with permission. Copyright 2023 Wiley-VCH.

[a] X. Qi, D. Liu, H. Yu, Z. Fu, Y. Zhang

Key Laboratory of Bio-inspired Smart Interfacial Science and Technology of Ministry of Education, School of Chemistry, Beihang University, Xueyuan Road 37, Beijing 100191, P. R. China

E-mail: liudp@buaa.edu.cn  
jade@buaa.edu.cn

[b] Y. Zhang

Beijing Advanced Innovation Center for Biomedical Engineering, Beihang University, Xueyuan Road 37, Beijing 100191, P. R. China

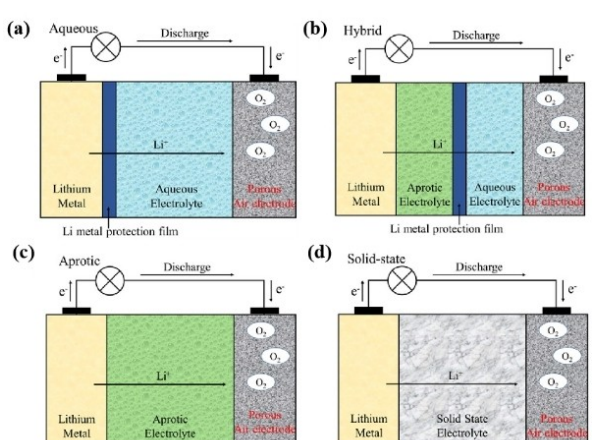


Figure 2. Schematic cell configurations for the four types of LABs. Reprinted from Ref. [11] with permission. Copyright 2014 American Chemical Society.

performance, and the ceramic electrolyte membranes are expensive for applications.<sup>[14]</sup> In comparison, non-aqueous LABs (Figure 2c) have a simpler battery structure and higher energy density,<sup>[15]</sup> however, non-aqueous electrolytes are flammable and volatile, showing poor compatibility with anodes and narrow electrochemical windows.<sup>[16]</sup> During cycling, it tends to produce Li dendrites, which will penetrate the separator and cause short circuits to significantly threaten battery safety and reduce cycle life.<sup>[17]</sup> As well, non-aqueous electrolytes are highly susceptible to attack by  $O_2^-$  leading to the formation of insulating byproducts and increased overpotentials.<sup>[18]</sup> Thus, it is evident that all of the three kinds of liquid electrolytes face insoluble challenges in terms of safety and stability, which strongly limits their further development. Another promising strategy is to replace liquid electrolytes with solid ones to construct all-solid-state LABs (ASSLABs) (Figure 2d).<sup>[19]</sup> Solid-state electrolytes (SSEs) have several advantages that (1) Battery combustion and explosion could be greatly eliminated arising from organic liquid leakage and volatility; (2) It will effectively protect Li anodes from corrosion by gases such as  $H_2O$  and  $CO_2$  in favor of long-term operation in air; (3) They can inhibit Li dendrites and electrolyte decomposition caused by nucleophilic intermediate attacks.<sup>[5,20]</sup> Nevertheless, there still exist urgent bottlenecks for SSEs, including low intrinsic ion conductivity and poor interface contact with electrodes.<sup>[21]</sup> Herein, this contribution reviews recent research progresses on SSEs for LABs in recent years to provide a detailed introduction to different types of SSEs, and more importantly the common issues regarding the interface contact between SSEs and electrodes. As well, we will summarize the prevailing design approaches and provide an outlook on their future development.

## 2. Solid-State Electrolytes

The earliest proposal of SSEs could be traced back to the early 20th century, which is primarily focused on inorganic materials such as oxides, sulfides, and nitrides.<sup>[22]</sup> In 1960, the solid-state ionic conductor material  $Ag_3Si$  was discovered and successfully applied to energy storage.<sup>[23]</sup> With the continuous advancement of research, it has opened a new era in SSEs since the discovery of  $\beta$ -alumina ( $Na_2O_{11}Al_2O_3$ ) that exhibits excellent ion conductivity at high temperatures and has been used in high-temperature sodium-sulfur batteries.<sup>[24]</sup> Afterwards, research on solid electrolytes has no longer been limited to inorganic materials. The field of SSE research expanded with the discovery of ionic transport in a solid polymer material based on poly(ethylene oxide) (PEO).<sup>[25]</sup> So far, SSEs can be classified into three categories: ceramic electrolytes (CEs), solid polymer electrolytes (SPEs), and composite solid electrolytes (CSEs).<sup>[26]</sup>

### 2.1. Ceramic Electrolytes

Metal sulfides and oxides are the most typical two kinds of CEs. Sulfide CEs mainly include the glass ceramic state  $Li_7P_3S_{11}$  (LPS), tetragonal state  $Li_{10}GeP_2S_{12}$  (LGPS) and  $Li_{9.54}Si_{1.74}P_{1.44}S_{11.7}C_{10.3}$  (LSPSC),<sup>[27]</sup> which have several advantages such as good compatibility with Li metal anodes, high ion conductivity, and wide electrochemical window. However, their sensitivity to water in air will lead to generation of toxic  $H_2S$  gas, so an inert atmosphere is often required for preparation and storage of samples. The inconvenience especially for outdoor use greatly limits the application of LABs.<sup>[18]</sup> While oxide CEs mainly include sodium superionic conductor (NASICON), garnet, perovskites, anti-perovskites, and zeolites.<sup>[28]</sup> Compared to sulfides, they have better chemical stability in open air and superior mechanical strength,<sup>[5]</sup> which have been employed for developing SSLABs. Several typical crystal structures of solid inorganic



Xianhai Qi is currently a graduate student at the School of Chemistry, Beihang University. His current research interests primarily focus on optimization and design of electrolytes for lithium-air batteries.



Yu Zhang received his Ph.D. degree from Jilin University in 2007. Then, he worked as a New Energy and Industrial Technology Development Organization fellow at Hiroshima University, Japan. He joined Beihang University in 2013 and now is a full professor of the School of Chemistry. He has worked for over 11 years in advanced energy materials, especially for optimizing electrode structures in the Li-air and Li/Na-ion battery field.



Dapeng Liu received his Ph.D. degree from Jilin University in 2008. During 2008–2012, he finished his postdoctoral research and worked as an associate professor at Changchun Institute of Applied Chemistry, Chinese Academy of Sciences. Then, he joined the School of Chemistry, Beihang University in 2013. His research mainly focuses on inorganic energy and catalytic materials.

electrolytes are displayed in Figure 3. In the following sections, we will focus on discussing the applications of oxide CEs.

### 2.1.1. Sodium Superionic Conductor

In 1976, Goodenough and coworkers reported the first NASICON-type structured solid electrolyte of  $\text{Na}_{1+x}\text{Zr}_2\text{P}_{3-x}\text{Si}_x\text{O}_{12}$  with three-dimensional (3D)  $\text{Na}^+$  channels.<sup>[28]</sup> Replacing  $\text{Na}^+$  with  $\text{Li}^+$  yields a NASICON solid electrolyte capable of conducting  $\text{Li}^+$ , and the chemical composition is generally described as  $\text{LiM}_2(\text{PO}_4)_3$  ( $\text{M}=\text{Ti, Ge, Zr}$ ).<sup>[29]</sup> However,  $\text{LiM}_2(\text{PO}_4)_3$  is of low  $\text{Li}^+$  conductivity,<sup>[30]</sup> and it needs to dope trivalent metal ions to partially replace tetravalent ones. As reported, doping  $\text{LiTi}_2(\text{PO}_4)_3$  with  $\text{Al}^{3+}$  to obtain  $\text{Li}_{1+x}\text{Al}_x\text{Ti}_{2-x}(\text{PO}_4)_3$  (LATP) could result in a  $\text{Li}^+$  conductivity of up to  $7 \times 10^{-4} \text{ S cm}^{-1}$  at room temperature when  $x=0.3$ .<sup>[31]</sup> Based on this, Zhao et al. designed a novel SSLAB that comprises a thinner electrolyte layer of LATP and a highly porous cathode (with porosity of 78%), both contributing to significantly reducing internal resistance while increasing the three-phase boundary. The battery could thus exhibit a discharge capacity as high as  $14200 \text{ mAh g}_{\text{carbon}}^{-1}$  at the current density of  $10 \text{ Ma cm}^{-2}$ .<sup>[32]</sup> However,  $\text{Ti}^{4+}$  is prone to be reduced to  $\text{Ti}^{3+}$  when in direct contact with Li metal, so they have tried to further dope inert  $\text{Ge}^{4+}$  to achieve a wide electrochemical window, and the synthesized  $\text{Li}_{1+x}\text{Al}_x\text{Ge}_{2-y}(\text{PO}_4)_3$  (LAGP) has been proved to be more stable toward Li metal.<sup>[18]</sup> The LAGP SSE performed well after assembled with plasmonic air electrode and Li metal anode into solar-driven SSLABs. Under the current density of  $400 \text{ mA g}^{-1}$  at the capacity limitation of  $1000 \text{ mAh g}^{-1}$ , the battery could stably work for 15 cycles at  $-73^\circ\text{C}$ , and more than 50 cycles at room

temperature.<sup>[33]</sup> Additionally, recent researchers have prepared a Zn-doped LATP solid electrolyte using a high-temperature solid-state method. The large ionic radius and high electronegativity of  $\text{Zn}^{2+}$  partially replaced the unstable  $\text{Ti}^{4+}$ , resulting in a denser crystal structure for the CE and enhancing its ionic conductivity. At the room temperature, its ionic conductivity reaches  $2.45 \times 10^{-3} \text{ S cm}^{-1}$ .<sup>[34]</sup> This doping strategy also offers a practical approach for achieving high-performance SSLABs.

### 2.1.2. Garnet-Type Electrolytes

In 2003, Thangadurai and coworkers firstly reported the garnet-type Li-ion conductor of  $\text{Li}_5\text{La}_3\text{M}_2\text{O}_{12}$  ( $\text{M}=\text{Nb, Ta}$ ),<sup>[35]</sup> and then the garnet-type SSE  $\text{Li}_7\text{La}_3\text{Zr}_2\text{O}_{12}$  (LLZO) was proposed in 2007 by Murugan et al. It is found that the thin LLZO sheets fabricated at  $25^\circ\text{C}$  could exhibit a total conductivity reaching  $7.74 \times 10^{-4} \text{ S cm}^{-1}$ .<sup>[36]</sup> These compounds exhibit bulk conductivities of  $10^{-6} \text{ S cm}^{-1}$  at  $20^\circ\text{C}$  and their activation energies are 0.43 and 0.56 eV for  $\text{Li}_5\text{La}_3\text{Nb}_2\text{O}_{12}$  and  $\text{Li}_5\text{La}_3\text{Ta}_2\text{O}_{12}$ , respectively.<sup>[5]</sup> The chemical general formula of a garnet-type CE is  $\text{A}_3\text{B}_2\text{C}_3\text{O}_{12}$ , where  $\text{A}=\text{Ca, Mg, La}$ ;  $\text{B}=\text{Al, Fe, Ga, Mn, Ni, V}$ ;  $\text{C}=\text{Si, Ge, Al}$ .  $\text{B}_2\text{C}_3\text{O}_{12}$  is the main framework, in which A, B and C refer to eight, six, and four coordinated cation sites, respectively,<sup>[37]</sup> and it is found that this type of electrolyte possesses high ionic conductivity. However, they are highly sensitive to water and  $\text{CO}_2$  that will induce the formation of a  $\text{Li}_2\text{CO}_3$  passivation layer, resulting in large resistance between the garnet electrolyte and the electrode interface.<sup>[21]</sup> Dry polishing, wet polishing, or heat treatment can be used to remove  $\text{Li}_2\text{CO}_3$ , or a metal, metal oxide, or polymer-based intermediate layer can be introduced between the solid electrolyte and the Li anode to enhance the adhesion between the garnet electrolyte and the electrode, thereby reducing the interface resistance.<sup>[18]</sup> A layer-structured ceramic electrolyte (LLZTO) with a density as high as 99.6% was reported by using the hot-pressing sintering technique, while simultaneously employing garnet powder, LiTFSI, and activated carbon to form a SSLAB.<sup>[38]</sup> At room temperature, the electrolyte's ionic conductivity reaches as high as  $1.6 \times 10^{-3} \text{ S cm}^{-1}$ . At  $20 \text{ Ma cm}^{-2}$ , the cut-off discharge capacity is  $1000 \text{ mAh g}_{\text{carbon}}^{-1}$  (Figure 4a), and the battery can cycle 50 times while maintaining its initial capacity (Figure 4b). In addition, Yao et al. investigated a high-performance solid-state  $\text{Li-O}_2$  battery (SSLOB) integrated architecture, which is based on LLZTO and porous composite cathode (Figure 4c). Its unique internal structure effectively reduces the battery's interfacial impedance, providing abundant active sites at the three-phase boundary, thus enhancing electrochemical stability. The battery can deliver a complete discharge capacity of  $13.04 \text{ mAh cm}^{-2}$  and excellent cycling performance for up to 86 cycles.<sup>[39]</sup>

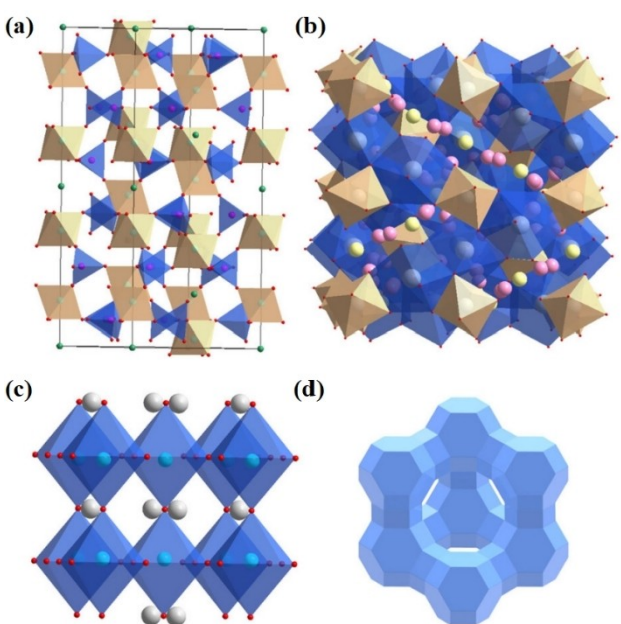


**Figure 3.** Several typical crystal structures of inorganic solid electrolytes: (a) NASICON-type LAGP, (b) Garnet-type LLZO, (c) Perovskite-type LLTO and (d) Zeolite X. Reprinted from Ref. [18] with permission. Copyright 2022 Wiley-VCH.

### 2.1.3. Perovskite and Anti-Perovskite Type Electrolytes

Perovskite materials are generally described as a structural formula of  $\text{ABO}_3$  ( $\text{A}=\text{Ca, Sr, La}$ ;  $\text{B}=\text{Al, Ti}$ ). Under different

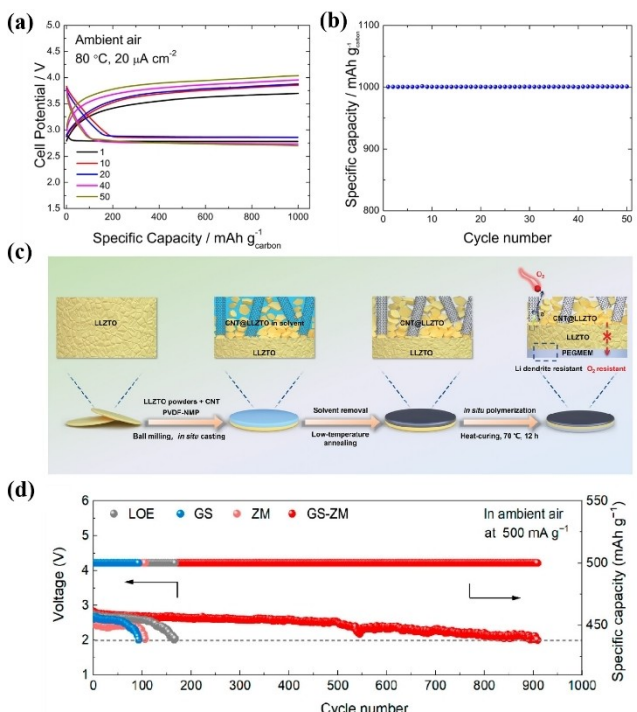


**Figure 4.** (a) The PPC:LiTFSI cell operated at 80 °C in real air with a cutoff discharge capacity of 1000 mAh g<sup>-1</sup> carbon at 20 μA cm<sup>-2</sup>. (b) The specific capacity as a function of cycle number. Reprinted from Ref. [38] with permission. Copyright 2017 Springer Nature. (c) Structure diagram of the LLZTO electrolyte with CNT@LLZTO cathode and PEGMEM buffer layer. Reprinted from Ref. [39] with permission. Copyright 2023 Wiley-VCH. (d) Cycling performance of LABs with LOE, GS, and SSLABs with ZM and GS-ZM at 500 mA g<sup>-1</sup>. Reprinted from Ref. [47] with permission. Copyright 2023 American Chemical Society.

synthetic conditions and doping concentrations, a variety of perovskites have been successfully prepared with different crystalline phases, including cubic, tetragonal, orthorhombic, and hexagonal ones.<sup>[40]</sup>  $\text{Li}_{3x}\text{La}_{(2/3)-x}\square_{(1/3)-2x}\text{TiO}_3$  ( $\square$  represents a vacancy) (LLTO) is a typical perovskite solid-state electrolyte. When  $x=0.11$ , it has a high ionic conductivity of approximately  $1\times 10^{-3}$  S cm<sup>-1</sup>, a wide electrochemical window, and high stability against Li metal.<sup>[37,41]</sup> However, their total ionic conductivity is relatively low due to the presence of grain boundary resistance in their structure.<sup>[42]</sup> Using the citrate-gel method, an Al-doped Li-La-Ti-O (A-LLTO) SSE was prepared by Park's group. SSEs assembled with this electrolyte operate stably in a pure O<sub>2</sub> atmosphere at temperatures from 25 to 100 °C and at the current density of 0.05 mA cm<sup>-2</sup>, delivering the first discharge from 796 mAh g<sub>C+CoO</sub><sup>-1</sup> to 4035 mAh g<sub>C+CoO</sub><sup>-1</sup>. Meanwhile, the improved A-LLTO exhibits a high ionic conductivity of  $3.17\times 10^{-4}$  S cm<sup>-1</sup>.<sup>[43]</sup> Nevertheless, the presence of Ti<sup>4+</sup> in LLTO renders it unstable upon contact with Li metal. By exchanging cations and anions in perovskite-type electrolytes, a novel anti-perovskite oxide can be obtained, which demonstrate enhanced stability towards Li metal and lower activation energies favorable for Li<sup>+</sup> migration, and show promising extensive applications in SSLABs.<sup>[44]</sup>

## 2.1.4. Zeolite-Type Electrolytes

Zeolites are a type of anionic aluminosilicates, consisting of silicon-oxygen tetrahedra and aluminum-oxygen tetrahedra as fundamental structural units, interconnected by oxygen bridge bonds to form regular pores or cages. Its unique microporous structure and continuous ion-conducting pathways within single crystals enable rapid migration of ions between crystals. Moreover, zeolites have good compatibility with air and Li metal, and can demonstrate excellent electrochemical stability in ambient air.<sup>[45]</sup> Yu et al. used lithium-ion-exchanged zeolite X (LiX) zeolite membrane (LiXZM) as inorganic SSE and carbon nanotubes (CNTs) as cathode to construct a highly stable flexible SSLAB. Via in situ assembly, a well-designed interface between SSE and cathode has been constructed, overcoming the issue of big contact resistance in traditional inorganic SSE batteries. In air, the discharge capacity could reach up to 12020 mAh g<sup>-1</sup> and stably cycle exceeding 149 times at the current density of 500 mA g<sup>-1</sup> and a fixed capacity of 1000 mAh g<sup>-1</sup>. Also this zeolite LAB demonstrates excellent flexibility and stability.<sup>[46]</sup> According to the "guest wrench" mechanism, they present an innovative ionic activation strategy by introducing a pair of cation and anion of LiTFSI-based guest species (GS) into the supercages to fabricate a zeolite membrane (ZM)-based solid electrolyte (GS-ZM) with high Li ionic conduction and interfacial compatibility. The restriction of zeolite frameworks is significantly reduced through the dynamic coordination of Li ions with the "oxygen wrench" of TFSI<sup>-</sup> at room temperature. GS-ZM shows ~100% increase in ionic conductivity compared with ZM and an outstanding Li<sup>+</sup> transference number of 0.97, and thus assembled ASSLAB could achieve a lifespan of 909 cycles at a current density of 500 mA g<sup>-1</sup> (Figure 4d).<sup>[47]</sup> The zeolite SSEs have shown great potential for application in other emerging energy storage systems such as Li-ion batteries, sodium-ion batteries, sodium-air batteries, zinc-air batteries, and so on.

In general, inorganic oxides such as NASICON, garnet, perovskite, anti-perovskite and zeolite are typical SSEs for LABs. Compared to perovskite and anti-perovskite electrolytes, NASICON and garnet-type electrolytes exhibit relatively higher ionic conductivity. While certain NASICON and garnet-type electrolytes still require exploration for improvement due to their instability towards air and Li metal. In addition, most ceramic electrolytes also face high grain boundary impedance, poor mechanical properties and other drawbacks. Improvements can be made through strategies such as elemental doping to optimize bottlenecks, constructing 3D ionic migration pathways, adjusting Li<sup>+</sup> or vacancy concentrations, and forming composite electrolytes. However, there is still a lack of guiding standards, and extensive research from both theoretical and experimental perspectives is needed for different crystal systems. Zeolites have a wide range of applications in SSLABs, and their successful implementation has opened new avenues for constructing practical SSEs with high Li<sup>+</sup> conductivity and intrinsic stability. However, it needs further investigation into the conductive behaviors associated with different cage sites

and the balance between mechanical strength and conductivity in zeolite SSEs.

## 2.2. Solid Polymer Electrolytes

In 1973, SPEs were first reported by P.V. Wright and colleagues, who found ionic conductivity in complexes of alkali metal salts with PEO.<sup>[48]</sup> SPEs are typically composed of low-molecular-weight polymer matrices such as PEO, PVDF, polyvinylidene fluoride-hexafluoropropylene (PVDF-HFP), polyacrylonitrile (PAN), poly (methyl methacrylate) (PMMA), and others. Compared to ceramics, solid polymer electrolytes exhibit better flexibility, processability, and operational safety.<sup>[49]</sup> However, polymer crystallization at room temperature slows down the dynamics of polymer segments, leading to relatively lower ionic conductivity.<sup>[50]</sup> This typically requires methods such as blending, copolymerization, cross-linking, adding plasticizers, directly increasing temperature, or preparing derivatives to enhance its conductivity.<sup>[51]</sup>

### 2.2.1. Polyethylene Oxide

PEO-based electrolytes, known for their excellent flexibility, viscoelasticity, low interfacial resistance, and manufacturing cost advantages, have attracted widespread attention.<sup>[52]</sup> As reported, the plasticized PEO-based solid electrolyte (PPE) (Figure 5a) could exhibit a conductivity of approximately  $10^{-3}$  S cm<sup>-1</sup> (Figure 5b) at room temperature. This is because during the plasticization process, the significantly decreased melting enthalpy of PPE leads to a notable reduction in membrane crystallinity and the enhancement of the conductivity of PPE, especially at lower temperatures. The LOB assembled with PPE exhibits excellent performance in terms of transport capacity, with a discharge capacity of up to 25 Ah g<sup>-1</sup> (12.5 mAh cm<sup>-2</sup>). XRD analysis confirms the reversibility of Li peroxide formation and dissolution during battery operation (Figure 5c). After optimization, the actual battery energy density can exceed 300 Wh kg<sup>-1</sup> (the theoretical value of 1350 Wh kg<sup>-1</sup>), which is twice than that of Li-ion batteries (Figure 5d).<sup>[53]</sup> Harding et al. investigated the stability of LABs by using PEO-based polymer electrolytes. The results indicate that PEO is prone to auto-oxidation in oxidative environments, severely impacting cycling efficiency, and moreover the solid-solid

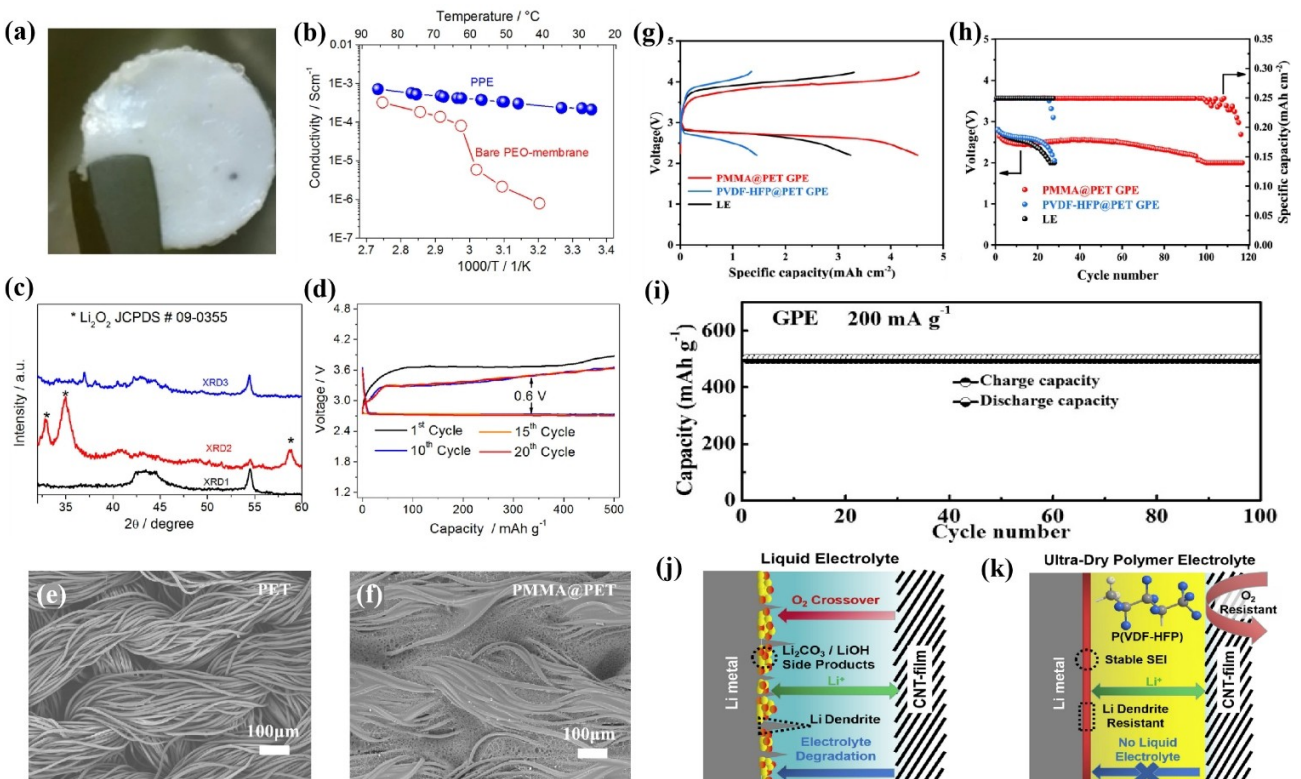


**Figure 5.** (a) The image of PPE. (b) Arrhenius plots of bare  $\text{PEO}_{20}\text{LiCF}_3\text{SO}_3\text{-ZrO}_2$  membrane (red curves) and PPE (blue curves). (c) X-ray diffraction patterns of the  $\text{Li}_2\text{O}_2$  deposition during LOB operation collected at the pristine state of the cell (black curves, XRD1), after full discharge (red curves, XRD2) and full charge (blue curves, XRD3). (d) Voltage profiles of the galvanostatic cycling test performed using a lithium oxygen polymer cell operating at controlled capacity regime by applying a  $100 \text{ mA g}^{-1}$  current with capacity limited to  $500 \text{ mAh g}^{-1}$ . Reprinted from Ref. [53] with permission. Copyright 2015 Springer Nature. (e) SEM diagram of PET fabric. (f) SEM diagram of PMMA@PET. (g) Voltage profiles of LOBs using PMMA@PET GPE as electrolytes at  $0.05 \text{ mA cm}^{-2}$ . (h) Discharge voltage plateaus (left axis) and charge capacities (right axis) of LOBs during cycling using PMMA@PET GPE. Reprinted from Ref. [55] with permission. Copyright 2023 American Chemical Society. (i) Cyclic performance the LOB assembled with PMMA/Pt/SiO<sub>2</sub>/PP GPE at a fixed capacity of  $500 \text{ mAh g}^{-1}$ . Reprinted from Ref. [57] with permission. Copyright 2015 American Chemical Society. Comparative schematic illustration of LOBs with (j) liquid electrolytes and (k) UDPEs. Reprinted from Ref. [66] with permission. Copyright 2020 Elsevier B.V.

interface contact between SSEs and electrodes increases interface impedance. Thus, PEO-based electrolytes have not been considered as the optimal choice for SPEs in LABs.<sup>[54]</sup>

### 2.2.2. Polymethyl Methacrylate

As an amorphous thermoplastic polymer, polymethyl methacrylate (PMMA) has a unique structure that the spatial hindrance between adjacent methyl groups prevents molecules from packing closely in a crystalline manner. At the same time, the methyl and methoxy functional groups in the PMMA structure restrict nucleophilic attacks by superoxide radicals, exhibiting superior stability.<sup>[55]</sup> Additionally, it exhibits excellent compatibility with both positive and anode. A novel gel polymer electrolyte (PMMA/IL-GPE) containing PMMA and ionic liquids (ILs) has been designed using ultraviolet curing. It demonstrates high stability against superoxide molecules and non-volatile ILs. PMMA/IL-GPE not only possesses the excellent ion conductivity ( $0.92 \text{ mS cm}^{-1}$ ), the wide voltage window (stable until  $> 4.7 \text{ V}$ ) and superior leakproof property, but also effectively protects Li anode from  $\text{O}_2^-$  attacking.<sup>[56]</sup> However, the mechanical property of PMMA is poor, and it usually needs to combine with other materials to enhance the performance. Electrochemically stable polyethylene terephthalate (PET) fabric was introduced into PMMA, followed by swelling in a mixed solution of tetraethylene glycol dimethyl ether (TEGDME) and lithium trifluoromethanesulfonate (LiTFSI) to prepare a stable PMMA-based gel polymer electrolyte (PMMA@PET GPE) (Figure 5e, f).<sup>[55]</sup> Due to the mechanical strength and elasticity reinforced by PET fabric, the growth of Li dendrites is effectively suppressed. PMMA@PET GPE has exhibited a high Li ion conductivity of  $0.71 \text{ mS cm}^{-1}$  at  $25^\circ\text{C}$ , so the SSLOB using PMMA@PET GPE could achieve a high reversible capacity of  $4.51 \text{ mAh cm}^{-2}$  (Figure 5g) and 117 stable cycles (Figure 5h). Additionally, via the multi-component synergistic strategy, a novel and stable GPE material has been cleverly designed by incorporating a polypropylene (PP) mechanical framework. This material, PP-supported PMMA-blend-PS with doping nanofumed  $\text{SiO}_2$  balanced the pros and cons of various components in terms of mechanical and electrochemical properties. Batteries assembled with this composite GPE exhibited excellent cycling stability and safety, achieving 100 cycles in air at room temperature (Figure 5i).<sup>[57]</sup>

### 2.2.3. Polyacrylonitrile

Polyacrylonitrile (PAN) based polymer electrolytes exhibit excellent performance, such as high thermal stability, high ionic conductivity, and a wide electrochemical window.<sup>[58]</sup> Meanwhile, a pair of electrons on the N atoms in PAN can coordinate with  $\text{Li}^+$ , thereby promoting the dissociation of Li salts and increasing the concentration of  $\text{Li}^+$  in electrolyte.<sup>[59]</sup> Application of PAN in SSEs or GPEs not only facilitates the transport of  $\text{Li}^+$  but also suppresses the growth of Li dendrites.<sup>[60]</sup> However, PAN has high crystallinity, and its reactivity with Li metal increases

the interfacial resistance between electrolyte and electrode, resulting in degradation of battery performance. Mixing with inorganic nanoparticles such as  $\text{TiO}_2$ ,  $\text{SiO}_2$ , and  $\text{Al}_2\text{O}_3$  can reduce the crystallinity of PAN and enhance its thermal stability.<sup>[59]</sup> Arof and coworkers utilized calix<sup>6</sup> as filler to prepare PAN-EC-PC-LiBOB-Calix[6]arene GPE. The LAB using PAN-EC-PC-LiBOB-Calix[6]arene GPE achieved the discharge capacity of  $233 \text{ mAh g}^{-1}$ , higher than  $187 \text{ mAh g}^{-1}$  of the LAB using PAN-EC-PC-LiBOB GPE.<sup>[61]</sup> In addition, the crystallinity of PAN can be reduced by introducing the redox mediator tetrachloro-1,4-benzoquinone (tCl-pBQ). The redox mediator tCl-pBQ was introduced into PAN-based GPEs (PAN/tCl-pBQ GPE), which could accelerate the formation of the amorphous phase in the gel polymer electrolyte matrix. Compared to PAN GPE, LABs assembled with PAN/tCl-pBQ GPE exhibited a decreased charge voltage from  $4.2 \text{ V}$  to  $3.6 \text{ V}$ , leading to an approximately 10% improvement in round-trip efficiency. At room temperature, the ionic conductivity increases to  $12.5 \text{ mS cm}^{-1}$  compared to  $7.64 \text{ mS cm}^{-1}$  of PAN GPE.<sup>[62]</sup>

### 2.2.4. PVDF and Polyvinylidene Fluoride-Hexafluoropropylene

PVDF-based electrolytes are of good flexibility, mechanical strength, and thermal stability.<sup>[63]</sup> In addition, due to high dielectric constant ( $\epsilon=8.4$ ), they possess significant solubility for Li salts.<sup>[64]</sup> However, issues such as low ionic conductivity, high crystallinity, and less reaction sites restrict the application of PVDF-based electrolytes in LABs. Nevertheless, in copolymer PVDF-HFP, the  $\text{CF}_3$  pendant group in HFP monomers which is randomly mixed with the VDF monomers, would provide steric hindrance and lead to higher amorphicity.<sup>[65]</sup> Compared to PVDF, the better ionic conductivity and mechanical stability enable PVDF-HFP electrolytes to serve as an ideal electrolyte substrate. Nan et al. have prepared the free-standing Li-ion conductive ultra-dry polymer electrolytes (UDPEs) by a simple tape-casting and vacuum-drying method, which are more resistant to  $\text{O}_2$  crossover and Li dendrite penetration than liquid electrolytes (Figure 5j, k). Simultaneously, UDPEs induce the formation of a stable LiF containing SEI on anode, greatly alleviating side reactions caused by liquid electrolyte degradation. The cycle life of the UDPE-based catalyst-free LOBs under a high current density of  $0.4 \text{ mA cm}^{-2}$  is improved by more than twofold in comparison with that of the liquid electrolyte-based battery.<sup>[66]</sup> Due to the strong chemical affinity of PVDF-HFP with  $\text{Li}^+$ ,  $\text{Li}^+$  can be uniformly distributed in the GPE and at the interface with Li anode. This can alleviate the common "tip effect", thus enabling better Li deposition. The as-prepared PVDF-HFP GPE exhibits high ionic conductivity and low interfacial resistance. When applied in LOBs assembled with Ni foam@ $\text{Co}_3\text{O}_4$ -50RuO<sub>2</sub> air cathodes, it can work for 553 cycles, exhibiting an ultra-long cycle life for over  $1100 \text{ h}$  and superior stability.<sup>[67]</sup>

Overall, despite the drawbacks of SPEs, such as low Li ion conductivity due to crystallization, decomposition of the polymer matrix and others. The polymer structures can be optimized through blending, copolymerization, and crosslink-

ing, whose ion conductivity is able to be improved by using plasticizers and other additives.

### 2.3. Composite Solid-State Electrolytes

As mentioned above, both inorganic CEs and SPEs have their respective advantages and disadvantages. Inorganic CEs could exhibit superior ionic conductivity but poor compatibility with electrodes and thus large interfacial impedance, while SPEs possess excellent mechanical properties and dimensional stability but inferior ionic conductivity at room temperature and a narrow electrochemical window. In order to obtain ideal SSEs, composite solid-state electrolytes (CSEs) can be constructed by combining ceramics with polymers by virtue of their synergistic effects.

According to different filler and matrix contents, CSEs can be classified into three categories of "ceramic-in-polymer" (CIP), "polymer-in-ceramic" (PIC), and "intermediate". Among them, CIP-CSEs use ceramic as filler and polymer as matrix, where inorganic ceramic particles are well dispersed in polymer. As for PIC-CSEs, polymer could serve as filler and ceramics as matrix. When the content of polymers and ceramics is roughly the same, it is considered an intermediate structural CSE.<sup>[18]</sup> The high ionic conductivity of CIP-CSEs should be attributed to the ceramic components that reduce the crystallinity of polymers and form strong affinity with Li<sup>+</sup> via Lewis acid-base interactions.<sup>[26]</sup> However, their low ceramic content (~20 wt%) often leads to insufficient mechanical strength and hence poor dendrite resistance. In contrast, PIC-CSEs, containing a high ceramic component (~50 wt%), boast superior safety and adequate mechanical strength to combat Li dendrite formation, making them better suited for practical applications.<sup>[68]</sup>

Song et al. have successfully prepared a 3D and interconnected LLZO garnet network that uniformly accommodates PEO in the large porous structure to form a composite electrolyte (3D-CPE) (Figure 6a). Thus obtained 3D-CPEs can contribute much to Li<sup>+</sup> transference through the LLZO bulk phase and along the continuous PEO/LLZO interface, which exhibits a high ionic conductivity of  $9.2 \times 10^{-5} \text{ Scm}^{-1}$  in ambient air at room temperature. Moreover, the 3D-CPE based SSLAB delivers high efficiency under the cut-off capacity of  $300 \text{ mAh g}^{-1}$  for 50 cycles (Figure 6b), surpassing the traditional CPEs prepared by LLZO particles (Figure 6c).<sup>[69]</sup> To enhance battery safety and cycling performance, the CSE composed of a 3D porous garnet microstructure (PSSE) and GPE has been developed to ensure a high ionic conductivity ( $1.06 \times 10^{-3} \text{ Scm}^{-1}$ ), in which the 3D garnet microstructure could serve as a rigid backbone to suppress Li dendrites and the consecutive GPE in PSSE provide ionic highway (Figure 6d). The assembled SSLABs exhibit excellent electrochemical performance that they can cycle 194 times without capacity decay at a high specific capacity of  $1250 \text{ mAh g}^{-1}$ , far surpassing pure GPEs (Figure 6e).<sup>[70]</sup> Afterwards, Zhang's group designed a CSE that consists of a rigid LAGP core and soft PVDF-HFP shell. The PVDF-HFP CSE ensures good interfacial contact between electrode and electrolyte, while LAGP guarantees sufficient hardness of the electrolyte to prevent penetration by Li dendrites. Finally, the SSLAB realized 146 cycles at  $300 \text{ mA g}^{-1}$  and  $1000 \text{ mAh g}^{-1}$  (Figure 6f).<sup>[71]</sup>

As for PIC electrolytes, they still face two challenges that significantly impact the mechanical properties and ionic conductivity: (1) Ceramic aggregation makes it difficult to establish a broad and continuous ceramic-polymer interface;<sup>[72]</sup> (2) The ceramic-polymer interface is unresponsive to conducting ions due to its inherent incompatibility.<sup>[73]</sup> It is an effective strategy to introduce polymer-compatible ionic liquids (PCILs)

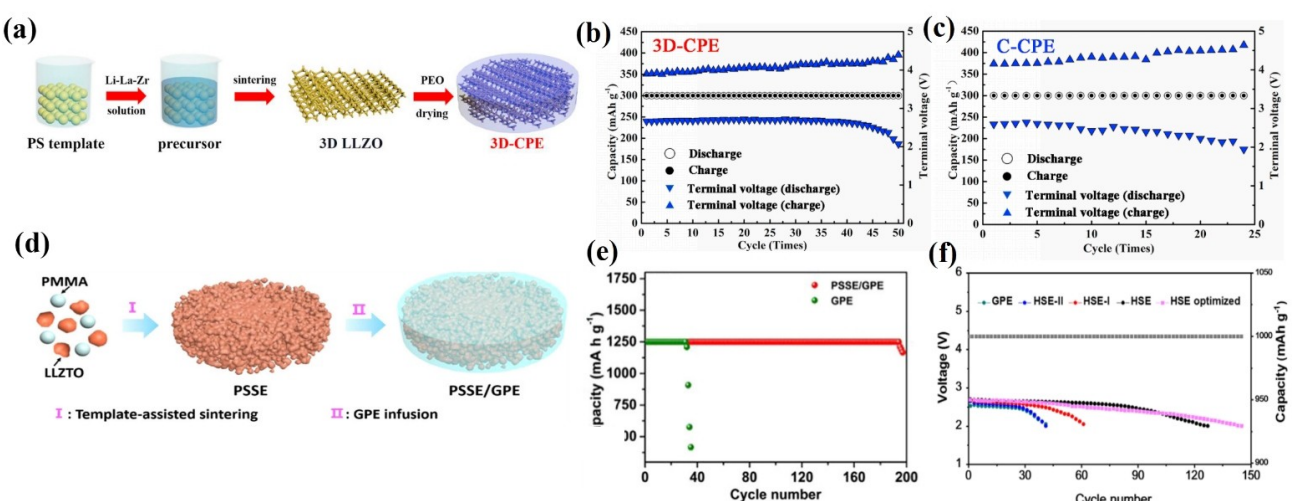


**Figure 6.** (a) Schematic demonstrating the preparation procedure for the composite polymer electrolyte with 3D LLZO network. (b–c) Discharge/charge voltage profiles of the LABs using 3D-CPE and C-CPE under a limited capacity cycling protocol of  $300 \text{ mAh g}^{-1}$ . Reprinted from Ref. [69] with permission. Copyright 2020 Elsevier B.V. (d) Schematic illustration for the synthesis of PSSE/GPE. (e) Cycling stability of LOBs with GPE and PSSE/GPE, respectively, with a limited capacity of  $1250 \text{ mAh g}^{-1}$  at a current density of  $312.5 \text{ mA g}^{-1}$ . Reprinted from Ref. [70] with permission. Copyright 2020 American Chemical Society. (f) Cycling stability of LOBs with different electrolytes, respectively, with a limited capacity of  $1000 \text{ mAh g}^{-1}$  at a current density of  $300 \text{ mA g}^{-1}$  (Among them, pink represents the formed composite solid electrolyte). Reprinted from Ref. [71] with permission. Copyright 2020 Oxford University Press on behalf of China Science Publishing & Media Ltd.

as mediator between ceramics and polymer matrices. The polar groups of PCILs interact with  $\text{Li}^+$  on the ceramic surface and polymer chain segments, resolving ceramic aggregation issues. Simultaneously, it activates the ceramic-polymer interface by establishing interpenetrating channels, facilitating efficient  $\text{Li}^+$  transport across the ceramic phase, ceramic-polymer interface, and spatial pathways. The PIC electrolyte (PELL60), consisting of 30 wt% PVDF as the conductive polymer matrix, 60 wt% PCIL-coated  $\text{Li}_3\text{Zr}_2\text{Si}_2\text{PO}_{12}$  (LZSP) ([EMIM][TFSI]@LZSP) as the ceramic filler, and 10 wt% of LiTFSI, was designed and prepared. At 25 °C, PELL60 exhibits a high ion conductivity of 0.83 mS cm<sup>-1</sup> and a stable electrochemical window of 5.01 V. Additionally, it has a  $\text{Li}^+$  migration number of 0.81 and an elongated capacity of ~300%.<sup>[74]</sup> This method effectively addresses the challenges of ceramic aggregation and ceramic-polymer interface in traditional composite SSEs, thus creating new opportunities for the development of composite SSEs suitable for LABs.

### 3. Interface Issues and Solutions

SSEs can address concerns regarding volatility and flammability. However due to their poor wettability, there is high interfacial resistance between the SSE and electrodes, which hinders the formation of efficient ion transport channels and satisfactory three-phase interfaces and hence slows down the reaction rate.<sup>[75b]</sup> The ideal interface between SSEs and electrodes should be as thin as possible and occupy only a small fraction of the battery volume so as to minimize interfacial impedance and slow down volume changes during cycling.<sup>[18]</sup>

#### 3.1. Physical Contact Modification

In SSLABs, the rigid physical contact between SSE and Li anode can easily lead to interface gaps, transforming the "surface" contact into "point" contact, and causing poor wetting at interface. To achieve ideal physical contact, the strategies by coating metal or metal oxide on the surface of Li anodes.<sup>[76]</sup> Similarly, point-to-point contact exists between the SSE and the cathode, resulting in excessively high local current density, which severely limits the high-rate charge and discharge performance. By using mixed electronic and ionic conductors, an air cathode of LOBs has been constructed. The face-to-face interface (Figure 7f) overcomes the limitations of the point-to-point ones (Figure 7a–e) and significantly enhances the electroactive surface area of electrode. This mixed conductor solid-state air cathode reduced the interface resistance, and the Coulombic efficiency of LOBs could be significantly improved from 38.6% to 80.8%.<sup>[77]</sup>

#### 3.2. Kinetics Enhancement

The interfacial kinetics of SSEs is unstable due to the presence of inhomogeneities, crystal defects, or material impurities, as well as crystal growth and defects that occur during use. The

transport of Li ions can be effectively promoted by introducing SSEs with doped redox mediators at interface or by embedding ion conductors on cathode. This approach improves the oxygen reduction reaction (ORR) and oxygen evolution reaction (OER) kinetics in SSLABs during charge/discharge.<sup>[29]</sup> A novel tert-butylmethoxyphenyl bromosilane (TBMPsiBr) was applied as an organic-inorganic CSE interphase-forming agent and a redox mediator for LOBs. At the current density of 1000 mA h g<sup>-1</sup>, LOBs containing LiBr exhibited rapid polarization after 80 cycles, with a sharp increase in charge-discharge overpotential. However in contrast, LOBs containing TBMPsiBr not only showed lower charge-discharge overpotential but also maintained discharge overpotential above 2.71 V after 220 cycles, significantly enhancing the electrochemical performance.<sup>[78]</sup>

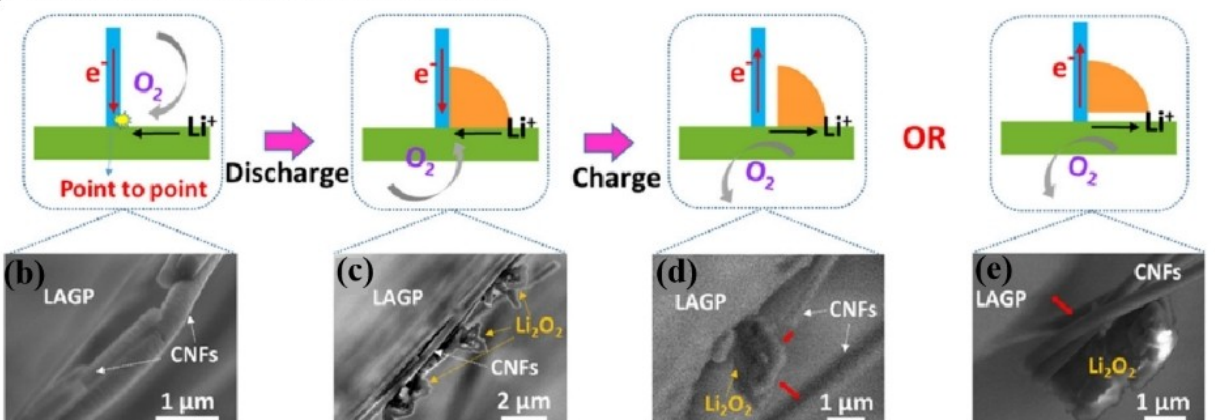
#### 3.3. Integrated Design

By employing an *in situ* integrated approach to introduce SSE onto the surface of porous cathodes, it ensures good contact at the solid-solid interface between electrolyte and electrode, ensuring good gas diffusion and facilitating the transport of Li ions and electrons. By sintering LATP/carbon source spheres, a novel SSLOB with an integrated electrolyte and cathode structure was developed by Zhao's team. The novel battery used a thinner electrolyte layer (approximately 10% thickness of traditional batteries) and a highly porous cathode (78% in porosity), significantly reducing the internal resistance while increasing the three-phase boundary. At a current density of 0.15 mA cm<sup>-2</sup>, the battery achieved a discharge capacity of up to 14,200 mA h g<sup>-1</sup> carbon and sustained 100 cycles at a fixed capacity of 1000 mA h g<sup>-1</sup> carbon.<sup>[32]</sup> In addition, Zhang et al. successfully prepared a porosity-adjustable plastic crystal electrolyte (PCE) using the thermally induced phase separation (TIPS) technique. They also introduced porous succinonitrile-based plastic crystal electrolytes (SLPB) *in situ* on the surface of carbon nanotube cathodes to form a continuous and enriched three-phase interface so as to ensure rapid flow of O<sub>2</sub> and Li<sup>+</sup> migration (Figure 7g). Thus assembled LOBs exhibited a high discharge capacity of 5963 mA h g<sup>-1</sup> and the cycling life up to 130 cycles at 32 °C (Figure 7h). Comparative experiments with carbon nanotubes as cathode confirmed the critical role of the three-phase boundary formed by the integrated design in battery capacity.<sup>[79]</sup>

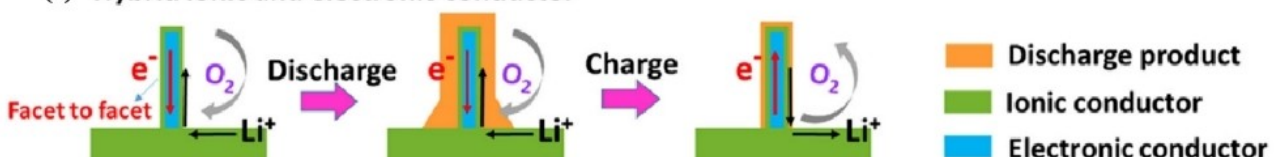
#### 3.4. Solvent-Induced Structural Modulation

The interface between electrolyte and electrode is closely related to the solvation structure of Li<sup>+</sup>. The interactions among Li<sup>+</sup>, solvents, and anions directly determine the solvation structure in the electrolyte solution.<sup>[10a]</sup> When the interaction between Li<sup>+</sup> and solvent is much greater than that between Li<sup>+</sup> and anions, the strong interaction between Li<sup>+</sup> and solvent molecules will dominate the solvation structure of Li<sup>+</sup>. Consequently, the resulting SEI rich in organic compounds typically leads to high Li<sup>+</sup> diffusion barriers and uneven Li<sup>+</sup> flux

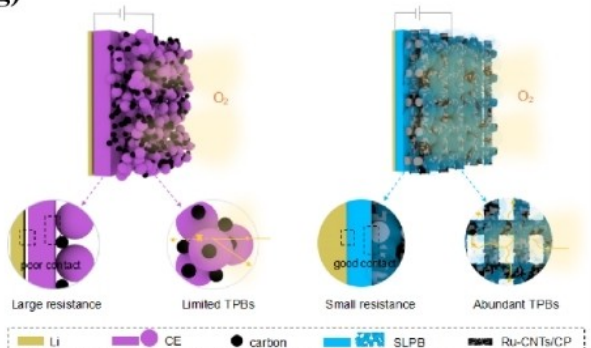
**(a) Mixed ionic and electronic conductors**



**(f) Hybrid ionic and electronic conductor**



**(g)**



**(h)**

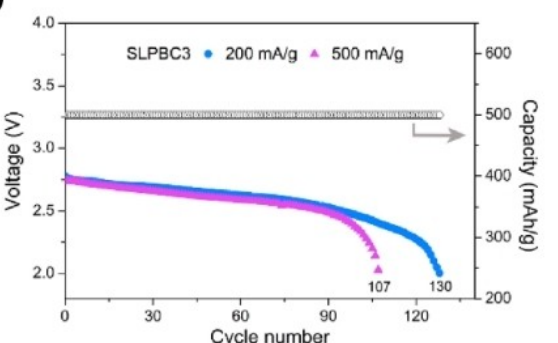


**Figure 7.** (a) Schematic illustration of the interfacial changes occurred during discharge and charge process for the LOBs based on mixed ionic and electronic conductors. (b–e) SEM images of LAGP/CNFs air electrode at different discharge-charge states of (b) before discharging, (c) after discharging, (d), (e) after recharging. (f) Schematic illustration of the interfacial changes occurred during discharge and charge process for the LOBs based on hybrid ionic and electronic conductors. Reprinted from Ref. [77] with permission. Copyright 2020 Wiley-VCH. (g) Schematic illustration of the conventional ASS LOB with CE and the ASS LOB with porosity-adjustable SLPB. (h) Cycling performance of the SSLOBs based on SLPB at 500  $\text{mA g}^{-1}$ . Reprinted from Ref. [79] with permission. Copyright 2020 Wiley-VCH.

at the anode interface, thereby exacerbating  $Li^+$  dendrite growth. On the contrary, when the interaction between  $Li^+$  and solvent is much smaller than the interaction between  $Li^+$  and anions, the solvation structure of  $Li^+$  containing anions favors interface chemical reactions at anode, resulting in a chemically homogeneous and mechanically stable SEI rich in inorganic compounds. This promotes enhanced  $Li^+$  transport kinetics and achieves uniform  $Li^+$  deposition.<sup>[80]</sup> By regulating solvation structure and thus the chemically and mechanically stable SEI, we can reduce the continuous reduction decomposition of electrolyte at the electrode interface, thereby greatly improving the cycling stability of the battery. Recently, the application of metal-organic frameworks (MOFs) in SSEs has attracted widespread attention.<sup>[81]</sup> After introducing solid-phase MOF membrane into the electrolyte, the solvent molecules weakly coordinated with

$Li^+$  are unable to approach the cathode surface.  $Li^+$  interacts with the anions through electrostatic interactions, resulting in uniform  $Li^+$  deposition at the interface at high current densities.<sup>[82]</sup> Also, introducing polymer polar groups is an effective modification approach, which can interact with functional groups in the solvent or polar atoms in the anions to reduce the activity of free solvent and minimizing solvent decomposition. Yu et al. utilized a polar polymer network (PPN) to modify the surface of  $Li$  anode. The  $C\equiv N$  groups of PAN polymer chains can engage in dipole-dipole interactions with the  $C=O$  groups of carbonate solvents, effectively reducing the reactivity of the carbonate electrolyte. Meanwhile, PAN exhibits weak interactions with  $Li^+$  and  $TFSI^-$ , facilitating the formation of an anion-dominated inorganic SEI and ensuring the interface stability.<sup>[83]</sup>

**Table 1.** Performance overview on LABs with SSEs in recent years.

Type	Component	Ionic conductivity ( $\text{mS cm}^{-1}$ )	Operating atmosphere	Cycle life/cycle capacity ( $\text{mAh g}^{-1}$ )	Ref.
CE	$\text{Li}_{1.3}\text{Al}_{0.3}\text{Ti}_{1.7}(\text{PO}_4)_3$	-	Air or $\text{O}_2$	100/1000	[32]
CE	$\text{Li}_{1.5}\text{Al}_{0.5}\text{Ge}_{1.5}\text{P}_3\text{O}_{12}$	0.39	Air	50/1000	[33]
CE	$\text{Li}_{6.4}\text{La}_{3}\text{Zr}_{1.4}\text{Ta}_{0.6}\text{O}_{12}$	1.6	Air	50/1000	[38]
CE	$(\text{Li}_{0.33}\text{La}_{0.56})_{1.005}\text{Ti}_{0.99}\text{Al}_{0.01}\text{O}_3$	0.317	$\text{O}_2$	132/500	[43]
CE	LiXZM	0.27	Air	149/1000	[46]
CE	LiTFSI-EMIMTFSI/LiX	0.54	Air	909/1000	[47]
SPE	$\text{PEO}_{20}\text{LiCF}_3\text{SO}_3$	~1	$\text{O}_2$	20/500	[53]
SPE	$\text{P}(\text{EO})_{20}\text{LiTf}$	-	$\text{O}_2$	210/1000	[84]
GPE	PMMA/IL	0.92	$\text{O}_2$	120/1000	[56]
GPE	PMMA/PSt/SiO <sub>2</sub> /PP	0.127	Air	100/500	[57]
GPE	PAN-EC-PC-LiBOB- calix[6]arene	-	Air	5/40	[61]
GPE	PAN/tCl-pBQ	12.5	Air	100/500	[62]
SPE	PVDF	0.059	$\text{O}_2$	50/1000	[67]
SPE	P(VDF-HFP)	0.079	$\text{O}_2$	60/1000	[67]
GPE	CA/P(VDF-HFP)	0.549	$\text{O}_2$	30/5000	[85]
CSE	$\text{Li}_7\text{La}_3\text{Zr}_2\text{O}_{12}/\text{PEO}$	0.092	Air	50/300	[69]
CSE	$\text{Li}_{6.4}\text{La}_2\text{Zr}_{1.4}\text{Ta}_{0.6}\text{O}_{12}/\text{PMMA}$	1.06	$\text{O}_2$	194/1250	[70]
CSE	$\text{Li}_{1.5}\text{Al}_{0.5}\text{Ge}_{1.5}(\text{PO}_4)_3/\text{PVDF-HFP}$	-	$\text{O}_2$	146/1000	[71]

## 4. Summary and Outlook

In this review, we have introduced the basic structure, the development of SSEs, and the interface issues between SSEs and electrodes of LABs. Compared to traditional LABs with flammable organic electrolytes, SSLABs have significant advantages in safety and stability. Solid inorganic electrolytes such as NASICON, garnet, perovskite, and zeolite, as well as solid polymer electrolytes including PEO, PMMA, PAN, PVDF, and PVDF-HFP, and CSEs, are the most promising candidate materials. Table 1 presents the recent progress in the cases of SSEs for LABs, contrasting their component, ionic conductivity, operating atmosphere, and cycle life, aiming to facilitate a more intuitive comparison and enable a deeper understanding of the specific applications of various SSEs in LABs. SSLABs have made many breakthroughs, but their applications are not yet fully mature, and the interface issues between SSEs and electrodes still need to be addressed. Four solutions have been proposed that (a) Physical contact modification contains surface coating designs for uniform contact between ions and electronic conductors as well as using porous cathodes to ensure uniform physical contact; (b) Kinetics enhancement can be conducted by doping redox mediators to increase the ionic conductivity of SSEs; (c) In situ integration has been introduced to SSEs on the surface of porous cathodes; (d) Solvation structure control can be realized by utilizing pore size effects or modifying polymer polar groups to control the solvation structure of Li ions, thereby limiting the contact and reaction between solvents or anions and Li metal anodes. Despite of great improvement in electrochemical performance and safety, further exploration and characterization of interface reaction processes are still required during the cycling of SSLABs.

The future development of LABs can be approached from the following aspects: (1) Integration of multiple methods to address interface issues, enhance electrochemical performance, and achieve large-scale production of SSLABs. For example, employing methods such as *in situ* integration or physical contact modification to eliminate or reduce loss in physical contact, simultaneously enhancing their kinetics, and using efficient catalysts to accelerate ORR and OER reactions. (2) Combining experimental, theoretical calculations, and advanced characterization techniques to conduct systematic and in-depth research on reactions occurring on both sides of the electrode and SSE interface, determining the ion transport mechanism. (3) Compared to LOBs, the air environment of SSLABs is more complex, and contaminants such as  $\text{H}_2\text{O}$ ,  $\text{O}_2$ ,  $\text{CO}_2$ , and  $\text{N}_2$  can seriously affect battery performance. This can be addressed by introducing multifunctional thin intermediate layers with high barrier properties to ensure the stable operation of SSLABs in ambient air environments at room temperature. We believe that with the continuous advancement of research, SSLABs will achieve significant breakthroughs in the future. The commercialization of SSEs in areas such as electric vehicles, aerospace, and wearable devices will accelerate.

## Acknowledgements

This work was financially supported by the National Natural Science Foundation of China (Grant no. 51925202, U23A20575, and U22A20141).

## Conflict of Interests

The authors declare no conflict of interest.

**Keywords:** Li-air batteries • Solid-state electrolytes • Ceramic electrolytes • Solid polymer electrolytes • Composite solid-state electrolyte

- [1] J. Lenders, *Adv. Mater.* **2019**, *31*, 1807431.  
[2] A. Manthiram, L. Li, *Adv. Energy Mater.* **2014**, *5*, 140132.  
[3] M. M. Ottakam Thottil, S. A. Freunberger, Z. Peng, Y. Chen, Z. Liu, P. G. Bruce, *Nat. Mater.* **2013**, *12*, 1050–1056.  
[4] J. H. Kang, J. Lee, J. W. Jung, J. Park, T. Jang, H. S. Kim, J. S. Nam, H. Lim, K. R. Yoon, W. H. Ryu, I. D. Kim, H. R. Byon, *ACS Nano* **2020**, *14*, 14549–14578.  
[5] Y. Liu, P. He, H. Zhou, *Adv. Energy Mater.* **2017**, *8*, 170162.  
[6] T. Liu, S. Zhao, Q. Xiong, J. Yu, J. Wang, G. Huang, M. Ni, X. Zhang, *Adv. Mater.* **2023**, *35*, 2208925.  
[7] a) D. Aurbach, B. D. McCloskey, L. F. Nazar, P. G. Bruce, *Nat. Energy* **2016**, *1*, 16128; b) F. Wu, Y. Yu, *Joule* **2018**, *2*, 815–817.  
[8] X. Bi, Y. Jiang, R. Chen, Y. Du, Y. Zheng, R. Yang, R. Wang, J. Wang, X. Wang, Z. Chen, *Adv. Energy Mater.* **2023**, *14*, 2302388.  
[9] K. Chen, D.-Y. Yang, G. Huang, X.-B. Zhang, *Acc. Chem. Res.* **2021**, *54*, 632–641.  
[10] a) P. Xiao, X. Yun, Y. Chen, X. Guo, P. Gao, G. Zhou, C. Zheng, *Chem. Soc. Rev.* **2023**, *52*, 5255–5316; b) F. Xiao, Q. Bao, C. Sun, Y. Li, D. Cui, Q. Wang, F. Dang, H. Yu, G. Lian, *Adv. Energy Mater.* **2024**, *14*, 2303766.  
[11] J. Lu, L. Li, J. B. Park, Y. K. Sun, F. Wu, K. Amine, *Chem. Rev.* **2014**, *114*, 5611–5640.  
[12] P. Chen, F. Bai, J. W. Deng, B. Liu, T. Zhang, *Front. Chem.* **2022**, *10*, 1035691.  
[13] S. Ida, A. K. Thapa, Y. Hidaka, Y. Okamoto, M. Matsuka, H. Hagiwara, T. Ishihara, *J. Power Sources* **2012**, *203*, 159–164.  
[14] Y. Li, L. Liu, C. Liu, Y. Lu, R. Shi, F. Li, J. Chen, *Chem.* **2019**, *5*, 2159–2170.  
[15] Y. Wang, *Electrochim. Acta* **2012**, *75*, 239–246.  
[16] Z. Zhang, X. Xiao, X. Zhu, P. Tan, *Electrochem. Energy Rev.* **2023**, *6*, 18.  
[17] L. Liu, H. Guo, L. Fu, S. Chou, S. Thiele, Y. Wu, J. Wang, *Small* **2021**, *17*, 1903854.  
[18] H.-F. Wang, X.-X. Wang, F. Li, J.-J. Xu, *Small Sci.* **2022**, *2*, 2200005.  
[19] S. Song, D. Zhang, Y. Ruan, L. Yu, Y. Xu, J. Thokchom, D. Mei, *ACS Appl. Energ. Mater.* **2021**, *4*, 6221–6232.  
[20] S. Choudhury, S. Stalin, Y. Deng, L. A. Archer, *Chem. Mater.* **2018**, *30*, 5996–6004.  
[21] J. Lai, Y. Xing, N. Chen, L. Li, F. Wu, R. Chen, *Angew. Chem. Int. Ed.* **2020**, *59*, 2974–2997.  
[22] T. T. Vu, H. J. Cheon, S. Y. Shin, G. Jeong, E. Wi, M. Chang, *Energy Storage Mater.* **2023**, *61*, 102876.  
[23] B. Reuter, K. Hardel, *Die Naturwissenschaften* **1961**, *48*, 161.  
[24] G. Liu, J. Yang, J. Wu, Z. Peng, X. Yao, *Adv. Mater.* **2024**, *36*, 2311475.  
[25] D. E. Fenton, D. M. Parker, P. V. Wright, *Polymer* **1973**, *14*, 589.  
[26] K. Pan, M. Li, W. Wang, S. Xing, Y. Dou, S. Gao, Z. Zhang, Z. Zhou, *Green Energy & Environ.* **2023**, *8*, 939–944.  
[27] Q. Zhang, D. Cao, Y. Ma, A. Natan, P. Aurora, H. Zhu, *Adv. Mater.* **2019**, *31*, 1901131.  
[28] J. B. Goodenough, H. Y.-P. Hong, J. A. Caffaras, *Mater. Res. Bull.* **1976**, *11*, 203–220.  
[29] Y. Hou, Z. Chen, R. Zhang, H. Cui, Q. Yang, C. Zhi, *Exploration* **2023**, *3*, 20220051.  
[30] K. Kwatek, J. L. Nowiński, *Solid State Ionics* **2017**, *302*, 54–60.  
[31] K. M. Kim, D. O. Shin, Y.-G. Lee, *Electrochim. Acta* **2015**, *176*, 1364–1373.  
[32] X. B. Zhu, T. S. Zhao, Z. H. Wei, P. Tan, G. Zhao, *Energy Environ. Sci.* **2015**, *8*, 2782–2790.  
[33] H. Song, S. Wang, X. Song, J. Wang, K. Jiang, S. Huang, M. Han, J. Xu, P. He, K. Chen, H. Zhou, *Energy Environ. Sci.* **2020**, *13*, 1205–1211.  
[34] Q.-C. Zhu, J. Ma, J.-H. Huang, D.-Y. Mao, K.-X. Wang, *Chem. Eng. J.* **2024**, *482*, 148977.  
[35] V. Thangadurai, H. Kaack, W. J. F. Weppner, *J. Am. Ceram. Soc.* **2003**, *86*, 437–440.  
[36] R. Murugan, V. Thangadurai, W. Weppner, *Angew. Chem. Int. Ed.* **2007**, *46*, 7778–7781.  
[37] T. Lu, Y. Qian, K. Liu, C. Wu, X. Li, J. Xiao, X. Zeng, Y. Zhang, S. L. Chou, *Adv. Energy Mater.* **2024**, *14*, 2400766.  
[38] J. Sun, N. Zhao, Y. Li, X. Guo, X. Feng, X. Liu, Z. Liu, G. Cui, H. Zheng, L. Gu, H. Li, *Sci. Rep.* **2017**, *7*, 41217.  
[39] Z. Gu, X. Xin, Z. Xu, J. He, J. Wu, Y. Sun, X. Yao, *Adv. Funct. Mater.* **2023**, *33*, 2301583.  
[40] a) S.-J. Lee, J.-J. Bae, J.-T. Son, *J. Korean Phys. Soc.* **2019**, *74*, 73–77; b) Y. Zhao, L. L. Daemen, *J. Am. Chem. Soc.* **2012**, *134*, 15042–15047; c) Z. D. Hood, H. Wang, A. Samuthira Pandian, J. K. Keum, C. Liang, *J. Am. Chem. Soc.* **2016**, *138*, 1768–1771.  
[41] a) S. Stramare, V. Thangadurai, W. Weppner, *Chem. Mater.* **2003**, *15*, 3974–3990; b) P. Borštnar, G. Dražić, M. Šala, C.-A. Lin, S.-K. Lin, M. Spreitzer, N. Daneu, *ACS Nano* **2024**, *18*, 10850–10862.  
[42] Y. Ding, Y. Li, Z. S. Wu, *Battery Energy* **2022**, *2*, 20220014.  
[43] H. T. T. Le, D. T. Ngo, P. N. Didwal, J. G. Fisher, C.-N. Park, I.-D. Kim, C.-J. Park, *J. Mater. Chem. A* **2019**, *7*, 3150–3160.  
[44] Z. Deng, D. Chen, M. Ou, Y. Zhang, J. Xu, D. Ni, Z. Ji, J. Han, Y. Sun, S. Li, C. Ouyang, Z. Wang, *Adv. Energy Mater.* **2023**, *13*, 2300695.  
[45] Y. Li, L. Li, J. Yu, *Chem.* **2017**, *3*, 928–949.  
[46] X. Chi, M. Li, J. Di, P. Bai, L. Song, X. Wang, F. Li, S. Liang, J. Xu, J. Yu, *Nature* **2021**, *592*, 551–557.  
[47] X. Chi, M. Li, X. Chen, J. Xu, X. Yin, S. Li, Z. Jin, Z. Luo, X. Wang, D. Kong, M. Han, J. J. Xu, Z. Liu, D. Mei, J. Wang, G. Henkelman, J. Yu, *J. Am. Chem. Soc.* **2023**, *145*, 24116–24125.  
[48] D. E. Fenton, J. M. Parker, P. V. Wright, *Polymer* **1973**, *14*, 589.  
[49] T. Panneerselvam, A. Rajamani, N. Janani, R. Murugan, S. Sivaprakasam, *Ionics* **2023**, *29*, 1395–1406.  
[50] H. K. Tran, Y.-S. Wu, W.-C. Chien, S.-H. Wu, R. Jose, S. J. Lue, C.-C. Yang, *ACS Appl. Energ. Mater.* **2020**, *3*, 11024–11035.  
[51] C. Sun, Z. Wang, L. Yin, S. Xu, Z. A. Ghazi, Y. Shi, B. An, Z. Sun, H.-M. Cheng, F. Li, *Nano Energy* **2020**, *75*, 104976.  
[52] H. Li, X. Xu, F. Li, J. Zhao, S. Ji, J. Liu, Y. Huo, *Chem.* **2023**, *29*, e202204035.  
[53] G. A. Elia, J. Hassoun, *Sci. Rep.* **2015**, *5*, 12307.  
[54] J. R. Harding, C. V. Amanchukwu, P. T. Hammond, Y. Shao-Horn, *J. Phys. Chem. C* **2015**, *119*, 6947–6955.  
[55] Y. Lian, M. Li, Y. Gao, M. Zhao, J. Liu, L. Xiao, *ACS Appl. Energ. Mater.* **2023**, *6*, 11364–11375.  
[56] H. Zhao, X. Liu, Z. Chi, S. Chen, S. Li, Z. Guo, L. Wang, *Appl. Surf. Sci.* **2021**, *565*, 150612.  
[57] J. Yi, X. Liu, S. Guo, K. Zhu, H. Xue, H. Zhou, *ACS Appl. Mater. Interfaces* **2015**, *7*, 23798–23804.  
[58] Z. Zhang, L. Zhang, Y. Liu, T. Yang, Z. Wang, X. Yan, C. Yu, *J. Mater. Chem. A* **2019**, *7*, 23173–23181.  
[59] X. Wang, Y. Fang, X. Yan, S. Liu, X. Zhao, L. Zhang, *Polymer* **2021**, *230*, 124038.  
[60] O. V. Yarmolenko, A. V. Yudina, K. G. Khatmullina, *Russ. J. Electrochem.* **2018**, *54*, 325–343.  
[61] M. Z. Kufian, A. K. Arof, *Mater. Technol.* **2014**, *29*, A114–A117.  
[62] Y. B. Kim, I. T. Kim, M. J. Song, M. W. Shin, *J. Membr. Sci.* **2018**, *563*, 835–842.  
[63] S. Zhou, S. Zhong, Y. Dong, Z. Liu, L. Dong, B. Yuan, H. Xie, Y. Liu, L. Qiao, J. Han, W. He, *Adv. Funct. Mater.* **2023**, *33*, 2214432.  
[64] Y. B. Kim, I. T. Kim, M. J. Song, M. W. Shin, *Electrochim. Acta* **2016**, *210*, 821–828.  
[65] T. Liu, Z. Chang, Y. Yin, K. Chen, Y. Zhang, X. Zhang, *Solid State Ionics* **2018**, *318*, 88–94.  
[66] W. Yu, C. Xue, B. Hu, B. Xu, L. Li, C.-W. Nan, *Energy Storage Mater.* **2020**, *27*, 244–251.  
[67] C. Zhao, J. Liang, Q. Sun, J. Luo, Y. Liu, X. Lin, Y. Zhao, H. Yadegari, M. N. Banis, R. Li, H. Huang, L. Zhang, R. Yang, S. Lu, X. Sun, *Small Methods* **2018**, *3*, 1800437.  
[68] N. Zhang, G. Wang, M. Feng, L.-Z. Fan, *J. Mater. Chem. A* **2021**, *9*, 4018–4025.  
[69] S. Song, X. Qin, Y. Ruan, W. Li, Y. Xu, D. Zhang, J. Thokchom, *J. Power Sources* **2020**, *461*, 228146.  
[70] C. Zhao, Q. Sun, J. Luo, J. Liang, Y. Liu, L. Zhang, J. Wang, S. Deng, X. Lin, X. Yang, H. Huang, S. Zhao, L. Zhang, S. Lu, X. Sun, *Chem. Mater.* **2020**, *32*, 10113–10119.  
[71] J. Wang, G. Huang, J. M. Yan, J. L. Ma, T. Liu, M. M. Shi, Y. Yu, M. M. Zhang, J. L. Tang, X. B. Zhang, *Natl. Sci. Rev.* **2021**, *8*, nwaa150.  
[72] Z. Chen, G. T. Kim, J. K. Kim, M. Zarrabeitia, M. Kuenzel, H. P. Liang, D. Geiger, U. Kaiser, S. Passerini, *Adv. Energy Mater.* **2021**, *11*, 2101339.  
[73] A. I. Waidha, T. Ferber, M. Donzelli, N. Hosseinpourkahavaz, V. Vanita, K. Dirnberger, S. Ludwigs, R. Hausbrand, W. Jaegermann, O. Clemens, *ACS Appl. Mater. Interfaces* **2021**, *13*, 31111–31128.

- [74] L. Zhu, J. Chen, Y. Wang, W. Feng, Y. Zhu, S. F. H. Lambregts, Y. Wu, C. Yang, E. R. H. van Eck, L. Peng, A. P. M. Kentgens, W. Tang, Y. Xia, *J. Am. Chem. Soc.* **2024**, *146*, 6591–6603.
- [75] a) L. Zhao, Y. Peng, F. Ran, *Energy Storage Mater.* **2023**, *58*, 48–73; b) S. S. Shinde, N. K. Wagh, S. H. Kim, J. H. Lee, *Adv. Sci.* **2023**, *10*, 2304235.
- [76] a) K. K. Fu, Y. Gong, B. Liu, Y. Zhu, S. Xu, Y. Yao, W. Luo, C. Wang, S. D. Lacey, J. Dai, Y. Chen, Y. Mo, E. Wachsman, L. Hu, *Sci. Adv.* **2017**, *3*, e1601659; b) X. Han, Y. Gong, K. K. Fu, X. He, G. T. Hitz, J. Dai, A. Pearse, B. Liu, H. Wang, G. Rubloff, Y. Mo, V. Thangadurai, E. D. Wachsman, L. Hu, *Nat. Mater.* **2017**, *16*, 572–579.
- [77] C. Zhao, Y. Zhu, Q. Sun, C. Wang, J. Luo, X. Lin, X. Yang, Y. Zhao, R. Li, S. Zhao, H. Huang, L. Zhang, S. Lu, M. Gu, X. Sun, *Angew. Chem. Int. Ed.* **2021**, *60*, 5821–5826.
- [78] C.-Y. Li, M.-S. Wu, W.-R. Chen, Q.-Y. Wang, Y.-J. Rong, X.-P. Zhang, *J. Mater. Chem. A* **2023**, *11*, 937–942.
- [79] J. Wang, G. Huang, K. Chen, X. B. Zhang, *Angew. Chem. Int. Ed.* **2020**, *59*, 9382–9387.
- [80] Y. Huang, J. Geng, Z. Jiang, M. Ren, B. Wen, J. Chen, F. Li, *Angew. Chem. Int. Ed.* **2023**, *62*, e202306236.
- [81] Y.-S. Wei, Z. Fan, C. Luo, S. Horike, *Nature Synthesis* **2023**, *3*, 214–223.
- [82] S. Bai, Y. Sun, J. Yi, Y. He, Y. Qiao, H. Zhou, *Joule* **2018**, *2*, 2117–2132.
- [83] J. Bae, Y. Qian, Y. Li, X. Zhou, J. B. Goodenough, G. Yu, *Energy Environ. Sci.* **2019**, *12*, 3319–3327.
- [84] M. Balaish, E. Peled, D. Golodnitsky, Y. Ein-Eli, *Angew. Chem. Int. Ed.* **2015**, *54*, 436–440.
- [85] L. Leng, X. Zeng, P. Chen, T. Shu, H. Song, Z. Fu, H. Wang, S. Liao, *Electrochim. Acta* **2015**, *176*, 1108–1115.

---

Manuscript received: September 21, 2024

Revised manuscript received: October 23, 2024

Accepted manuscript online: October 24, 2024

Version of record online: November 19, 2024

---